catalysts

MDPI

*Article*

# Nickel Phosphide Catalysts as Efficient Systems for $CO_2$ Upgrading via Dry Reforming of Methane

**Miriam González-Castaño [1,*], Estelle le Saché [2], Cameron Berry [2], Laura Pastor-Pérez [2], Harvey Arellano-García [1], Qiang Wang [3] and Tomás R. Reina [2,*]**

1 Department of Process and Plant Technology, Brandenburg University of Technology (BTU), Cottbus-Senftenberg, Platz der Deutschen 1, 03046 Cottbus, Germany; arellano@b-tu.de
2 Department of Chemical and Process Engineering, University of Surrey, Guildford GU2 7XH, UK; estelle.lesache@surrey.ac.uk (E.l.S.); cb00311@surrey.ac.uk (C.B.); l.pastorperez@surrey.ac.uk (L.P.-P.)
3 College of Environmental Science and Engineering, Beijing Forestry University, Beijing 100083, China; qiangwang@bjfu.edu.cn
* Correspondence: gonzalez@b-tu.de (M.G.-C.); t.ramirezreina@surrey.ac.uk (T.R.R.)

**Abstract:** This work establishes the primordial role played by the support's nature when aimed at the constitution of $Ni_2P$ active phases for supported catalysts. Thus, carbon dioxide reforming of methane was studied over three novel $Ni_2P$ catalysts supported on $Al_2O_3$, $CeO_2$ and $SiO_2$-$Al_2O_3$ oxides. The catalytic performance, shown by the catalysts' series, decreased according to the sequence: $Ni_2P/Al_2O_3$ > $Ni_2P/CeO_2$ > $Ni_2P/SiO_2$-$Al_2O_3$. The depleted $CO_2$ conversion rates discerned for the $Ni_2P/SiO_2$-$Al_2O_3$ sample were associated to the high sintering rates, large amounts of coke deposits and lower fractions of $Ni_2P$ constituted in the catalyst surface. The strong deactivation issues found for the $Ni_2P/CeO_2$ catalyst, which also exhibited small amounts of $Ni_2P$ species, were majorly associated to Ni oxidation issues. Along with lower surface areas, oxidation reactions might also affect the catalytic behaviour exhibited by the $Ni_2P/CeO_2$ sample. With the highest conversion rate and optimal stabilities, the excellent performance depicted by the $Ni_2P/Al_2O_3$ catalyst was mostly related to the noticeable larger fractions of $Ni_2P$ species established.

**Keywords:** $Ni_2P$; supported catalysts; dry reforming of methane; $Al_2O_3$; $CeO_2$; $SiO_2$-$Al_2O_3$

check for updates

**Citation:** González-Castaño, M.; le Saché, E.; Berry, C.; Pastor-Pérez, L.; Arellano-García, H.; Wang, Q.; Reina, T.R. Nickel Phosphide Catalysts as Efficient Systems for $CO_2$ Upgrading via Dry Reforming of Methane. *Catalysts* **2021**, *11*, 446. https://doi.org/10.3390/catal11040446

Academic Editor: Antonio Vita

Received: 15 March 2021
Accepted: 28 March 2021
Published: 30 March 2021



## 1. Introduction

The reduction of atmospheric carbon dioxide, and thus the greenhouse effect, is one of the defining scientific and engineering challenges of our time. Progress is being made in reducing carbon dioxide emissions, and technologies such as carbon capture and storage are available [1]. However, the sequestering of carbon dioxide in oceans or mineral formations is expensive and provides no useful end product. One technology with great potential in this field is the dry reforming of methane (DRM, $CO_2 + CH_4 = 2CO + 2H_2$) to produce a mixture of carbon monoxide and hydrogen—syngas. Dry reforming was first studied by Fischer and Tropsch as early as 1928 [2], and today attracts ever increasing interest due to the rising importance of $CO_2$ mitigation. The advantages of the dry reforming of methane are two-fold. Firstly, methane is also a potent greenhouse gas, so the reduction of this pollutant in the atmosphere is highly desirable. Secondly, the product syngas, as well as being a viable fuel for internal combustion [3], is an important feedstock for the production of higher hydrocarbon fuels through the Fischer Tropsch process [4] and for methanol production [5].

The DRM reaction is endothermic, requiring low pressure and high temperatures, above 600 °C according to thermodynamics, to progress at a good rate [6]. A significant amount of research has focused on noble metal catalysts. These catalysts often present far superior resistance to deactivation compared to transition metals. Still, the high cost of noble metals has driven research towards cost-effective formulations, usually based on transition metals such as Cu, Fe and Ni [2]. For traditional supported catalysts, deactivation issues related to carbon deposits, metal sintering and the oxidation of active species have been reported [7]. Compared to Fe and Co systems, relatively higher coking endurances coupled to fair reaction rates have been described for Ni catalysts. Over the past few decades, a substantial body of research has focused on reducing the deactivation of nickel catalysts by employing different metal oxide supports and metal promoters [1,2,6]. On developing effective catalysts, the rapid surface decomposition of methane, coupled with low tendencies towards constituting carbon deposits, potentially blocking the active sites, are generally intended features. On this premise, competitive catalytic systems have been reported. For instance, the Ni-Sn/$CeO_2$-$Al_2O_3$ catalyst combined the higher reaction rates depicted by Ni-Sn alloys with the benefits provided by oxygen vacancies of cerium dioxide support [8]. It is known that the support strongly determines the performance displayed by dry reforming catalysts, the metal support interfaces being described as powerful actives sites. Depositing catalytic material on a porous support also increases the metal exposed area whilst the acid-base support promotes $CH_4$/$CO_2$ activation, thus favouring the reaction rate [2]. For DRM reactions, it is known that relatively acidic supports such as $SiO_2$ favour the cracking of methane, which is usually considered as a rate limiting step. On the contrary, basic surfaces promote the activation of $CO_2$ molecules. In fact, oxygen vacancies present in partially reduced oxides have also been stated as effective sites towards $CO_2$ dissociative reductions [9]. Nevertheless, the acid base properties could also determine the extent of carbon deposits constituted over the catalyst surface [6].

When seeking novel catalyst formulations, transition metal carbides and phosphides have been proposed as appealing catalytic materials for a number of catalytic reactions, such as WGS and CO hydrogenation [10,11]. Among them, $Mo_2C$ catalysts are suggested as appealing alternatives, even being described as Pt-like materials [12,13]. In this context, Yao et al. [14] proposed molybdenum phosphide as a highly active and stable catalyst for dry reforming. Likewise, Guharoy et al. [15] proposed, via Density Functional Theory (DFT) calculations, nickel phosphide structures as active sites for Reverse Water Gas Shift (RWGS) reaction on the basis of the potential surface energies estimated for different reaction intermediates. Although scarcely analysed for $CO_2$ reduction processes, nickel phosphide clusters have proven successful as a catalyst for the hydrotreating of species such as thiophene [11]. For $Ni_2P$ surfaces, the strong oxygen interaction has been also related to promoted Water Gas Shift reaction rates [16] and hindered deactivation by coking in dry reforming applications [17]. Furthermore, the low barrier energy towards $H_2$ dissociation, along with the thermodynamic stability of H species over $Ni_2P$ surfaces under hydrogen rich environments, suggest $Ni_2P$ as an active phase for DRM reactions [18].

Considering the promising prospect envisaged for $Ni_2P$ active sites, this work aims to establish the influence of the support on $Ni_2P$ catalysts for DRM reactions. For that purpose, and in order to cover a wide range of chemical properties, 20% $Ni_2P$ was impregnated over $Al_2O_3$, $SiO_2$-$Al_2O_3$ and $CeO_2$ supports. From the obtained characterisation and activity outcomes, $Ni_2P$/$Al_2O_3$ catalysts could lead to a viable industrial $CO_2$ recycling process, with an impact on the pressing problem of rising atmospheric $CO_2$ levels.

## 2. Results and Discussion

### *2.1. Structural Characterization of the Samples*

The textural properties of the as-prepared mesoporous samples were evaluated by $N_2$-physisorption. Figure 1 displays the $N_2$ adsorption desorption hysteresis exhibited by the catalysts' series. According to IUPAC (International Union of Pure and Applied Chemistry) classification, the $Ni_2P$/$Al_2O_3$ and $Ni_2P$/$SiO_2$-$Al_2O_3$ samples presented a type H4 hysteresis shape characteristic of mesoporous materials. Considerably different hysteresis was noticed for the $Ni_2P$/$CeO_2$ system, which presented type H3 isotherm shapes usually associated to aggregated particles. Table 1 summarises the results of the BET and BJH analysis. Compared to $Ni_2P$/$Al_2O_3$ and $Ni_2P$/$SiO_2$-$Al_2O_3$ catalysts, significantly lower surface areas were discerned for the Ni/$CeO_2$ catalyst. Besides, the metal incorporation resulted in decreased surface areas and pore volumes for all the catalysts' series. The lower surface and pore volumes observed with respect to the supports are most likely associated with the presence of non-porous Ni particles which, at the same time, might be partially blocking the surface pores [19].

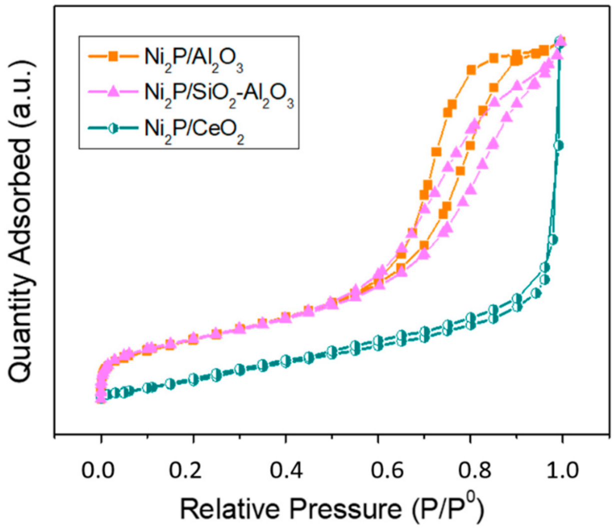


**Figure 1.** $N_2$ adsorption–desorption isotherms for the catalysts´ series.

**Table 1.** Textural properties of the prepared catalysts.

| Support | Surface Area ($m^2$/g) | $D_{pore}$ (nm) | $V_{pore}$ ($cm^3$/g) |
|---|---|---|---|
| $Al_2O_3$ | 202 | 7.4 | 0.51 |
| $SiO_2$-$Al_2O_3$ | 420 | 8.5 | 0.80 |
| $Ni_2P/Al_2O_3$ | 161 | 6.8 | 0.41 |
| $Ni_2P/CeO_2$ | 16 | 2.2 | 0.09 |
| $Ni_2P/SiO_2$-$Al_2O_3$ | 226 | 6.8 | 0.58 |

Figure 2 displays the diffractograms obtained for the as-prepared samples where $\gamma$-$Al_2O_3$ support (JCPDS No. 29-0063) is also included for clarity. For the $Ni_2P/Al_2O_3$ and $Ni_2P/SiO_2$-$Al_2O_3$ samples, no diffraction peaks associated to $AlPO_4$ or $NiAl_2O_4$ phases were observed. The constitution of $NiAl_2O_4$ phases could be restricted due to the relatively lower calcination temperatures (500 °C). Concerning the $Ni_2P/SiO_2$-$Al_2O_3$ sample, the relatively lower signal to noise ratio showed should be ascribed to the amorphous structure of silica present in the support (20% $SiO_2$) [20]. The characteristic peaks of fluorite $CeO_2$ (JCPDS No. 34-0394) were clearly observed for the $Ni_2P/CeO_2$ system.

Besides, no clear diffraction peaks associated to Ni phases were observed for any of the samples. Omar et al. [21] argued that nickel phosphate calcined up to 600 °C results in amorphous structures, whilst increasing the calcination temperature up to 900 °C permits the constitution of highly crystalline $Ni_2P$ phases. Thus, the lack of $Ni_2P$ peaks in XRD data should relate to the amorphous character of nickel phosphate deposits because of the employed calcination temperature.

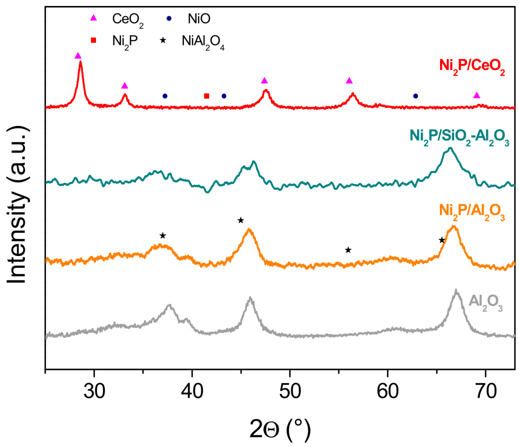


**Figure 2.** XRD diffractograms obtained for the catalysts' series.

### *2.2. Surface Characterization of the Samples: XPS Analysis*

Figure 3A shows the Ni $2p_{3/2}$ spectra obtained for reduced samples where $Ni^{\delta+}$ and $Ni^{2+}$ species along with their corresponding satellites are identified. For the $Ni_2P/Al_2O_3$ and $Ni_2P/SiO_2$-$Al_2O_3$ samples, the band contribution located at 852.7 eV was associated to $Ni^{\delta+}$ species. Slightly lower binding energies (852.5 eV) were observed for $Ni^{\delta+}$ species in the case of the $Ni/CeO_2$ catalyst. For Ni-supported ceria systems, peak shifts towards lower binding energies are usually related to the higher electron densities attained by Ni species in contact with partially reduced ceria support [22].

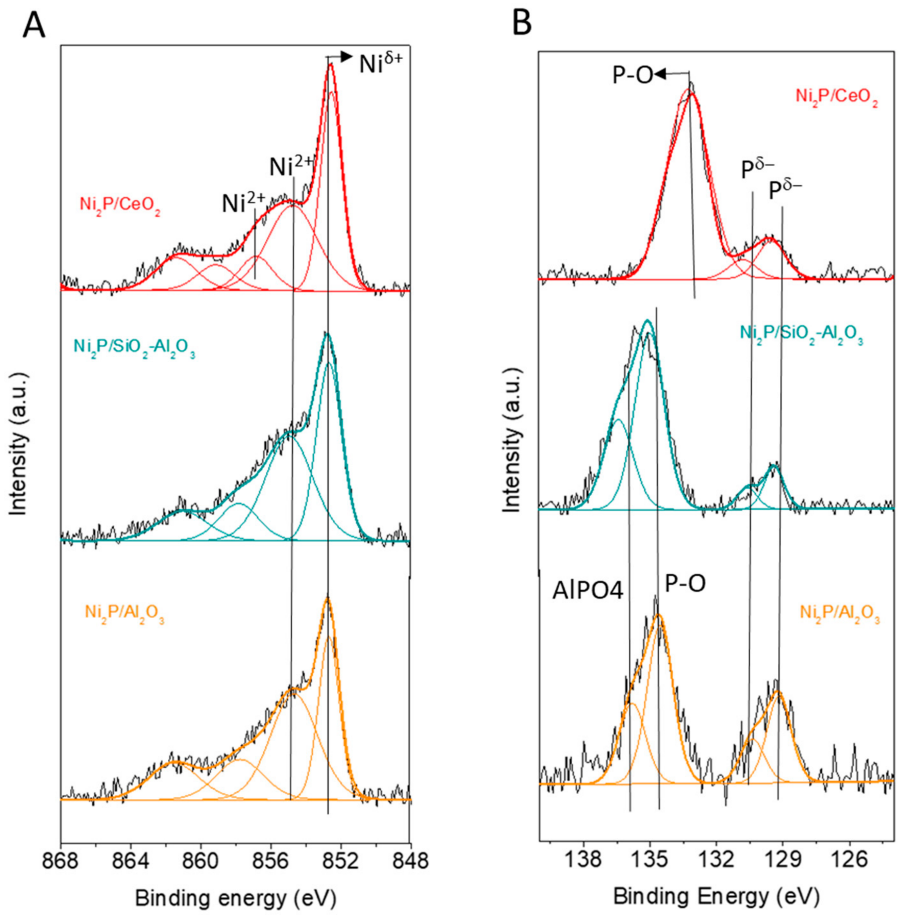


**Figure 3.** XPS spectra obtained for reduced samples: (**A**) Ni $2p_{3/2}$; (**B**) P 2p.

Besides, all samples exhibited peaks attributed to oxidised nickel species. Still, the support nature significantly influenced the electronic structure displayed by surface $Ni^{2+}$ species. Typically, bands located at 854.7 and 856 eV are assigned to NiO and $Ni(OH)_2$ species, respectively. For the reduced $Ni_2P/Al_2O_3$ and $Ni_2P/SiO_2$-$Al_2O_3$ samples, XPS data showed a single $Ni^{2+}$ band located at 854.7 and 855.0 eV, correspondingly. The differences observed for the $Ni^{2+}$ binding energies between the $Ni_2P/Al_2O_3$ and $Ni_2P/SiO_2$-$Al_2O_3$ samples underline the higher electronic density achieved for the $Ni_2P/Al_2O_3$ sample. Instead, two different peaks located at 854.7 and 856.8 eV were observed for $Ni/CeO_2$ catalyst, underlining two different $Ni^{2+}$ species interacting with partially reduced cerium dioxide.

In the P2p region (Figure 3B), bands associated to slightly negatively charged phosphorous species ($P^{\delta-}$) were discerned for all samples. Considering the $Ni^{\delta+}$ species noticed in the Ni $2p_{3/2}$ spectra, the presence of $Ni_2P$ surface clusters with the consequent electrons transfer from Ni to P species could be advocated [23]. Once again, the support nature influenced the electron properties exhibited by $P^{\delta-}$ surface species. Thus, while the $Ni_2P/Al_2O_3$ sample exhibited bands located at 129.2 and 130.4 eV, associated to $P^{\delta-}$ species, the larger binding energies noticed for $P^{\delta-}$ species in the $Ni_2P/SiO_2$-$Al_2O_3$ sample (129.4 and 130.6 eV) suggest that $P^{\delta-}$ species presented lower electron densities. This suggests that stronger Ni–P interactions and enhanced electron donations from Ni to P were achieved for the $Ni_2P/Al_2O_3$ sample. For the $Ni_2P/CeO_2$ system, $P^{\delta-}$ species appeared (129.5 and 133.0 eV) due to, in agreement with previous outcomes, efficient charge redistribution processes at the $Ni_2P$-$CeO_2$ interface [24].

Furthermore, the bands showing higher binding energies for all samples are usually ascribed to highly oxidized P species. In this sense, the bands located at 134.6 and 135.0 eV noticed for the $Ni_2P/Al_2O_3$ and $Ni_2P/SiO_2$-$Al_2O_3$ samples were ascribed to $P^{5+}$ species. For the $Ni_2P/CeO_2$ samples, $P^{5+}$ species appeared at significantly lower binding energies. For the latter systems, bands placed at 135.8 and 136.4 eV were ascribed to the constitution of $AlPO_4$ [25].

Therefore, all reduced catalysts displayed both $Ni^{2+}$ and Ni slightly oxidized ($Ni^{\delta+}$) species constituting $Ni_2P$ surface clusters, in agreement with the Ni $2p_{3/2}$ and P 2p spectra. The larger electron density displayed by $P^{\delta-}$ for the $Ni_2P/Al_2O_3$ catalyst suggested strongly interacting nickel phosphide structures. Besides, Ni particles interacting with cerium dioxide result in the evolution of: (i) rich-electron density $Ni^{\delta+}$ species and (ii) two different $Ni^{2+}$ species with relatively low electronic densities. The dispersion of the catalyst material on the supports was approximated by the atomic ratio of nickel species to support material on the catalysts' surfaces (Table 2). This calculation revealed that the ceria supported catalyst had the greatest proportion of its surface occupied by nickel species. Although strong Ni-ceria interactions and high metal dispersions are usually reported, this result can also be significantly influenced by the lower specific surface area of the ceria support. When comparing the alumina and silica-alumina supported catalysts, the higher Ni surface coverage found for the $Ni_2P/SiO_2$-$Al_2O_3$ sample suggests that the $SiO_2$-$Al_2O_3$ dispersing matrix favours, at least a priori, the Ni metal dispersion. For Ni supported catalysts, the optimal Ni loading over the $Al_2O_3$ and $ZrO_2$ dispersing matrix was found at 20 and 30%, respectively [26]. In agreement, the obtained outcomes suggest that silica-based supports lead to greater dispersion of the nickel species over the surface. From XPS data, the $Ni/Ni^{\delta+}$ surface ratio displayed by the catalyst series was also estimated. Qualitatively, the higher $Ni^{\delta+}/Ni^{2+}$ ratios found for the $Ni_2P/SiO_2$-$Al_2O_3$ sample might be associated to the higher dispersions. Besides, the significantly higher $P^{\delta-}/[P^{5+}$+P-O] ratios found over the $Ni_2P/Al_2O_3$ sample corroborated the favourable constitutions of $Ni_2P$ phases already intuited from the higher $P^{\delta-}$ electron densities noticed in the P 2p spectra.

**Table 2.** Surface composition of the catalysts as determined by XPS analysis, the atomic ratios of nickel to support material.

| Catalyst | Ni/Support | Ni Coverage (%) | $Ni^{\delta+}/Ni^{2+}$ | $P^{\delta-}/[P^{5+}+P\text{-}O]$ |
|---|---|---|---|---|
| $Ni_2P/Al_2O_3$ | 0.08 | 1.52 | 0.67 | 0.48 |
| $Ni_2P/SiO_2$-$Al_2O_3$ | 0.09 | 2.25 | 0.90 | 0.13 |
| $Ni_2P/CeO_2$ | 0.28 | 6.24 | 0.78 | 0.22 |

### 2.3. Catalytic Activity

Figure 4 shows the catalyst performance exhibited by the samples at 30 L/g·h and 700 °C. For all reaction tests, the $CH_4$ conversion was lower than the $CO_2$ conversion. This is congruent with the current literature on the kinetics and equilibrium of dry reforming of methane where the activation of $CH_4$ on the catalysts' surface is often cited as the rate limiting step for DRM [27]. Hence, the equilibrium conversion of $CO_2$ should be ca. 10% higher than for $CH_4$ [2]. Initially, all systems achieved close to 1 $H_2/CO$ ratios and, in the case of the $Ni_2P/CeO_2$ sample, decreased proportionally to the conversion rate.

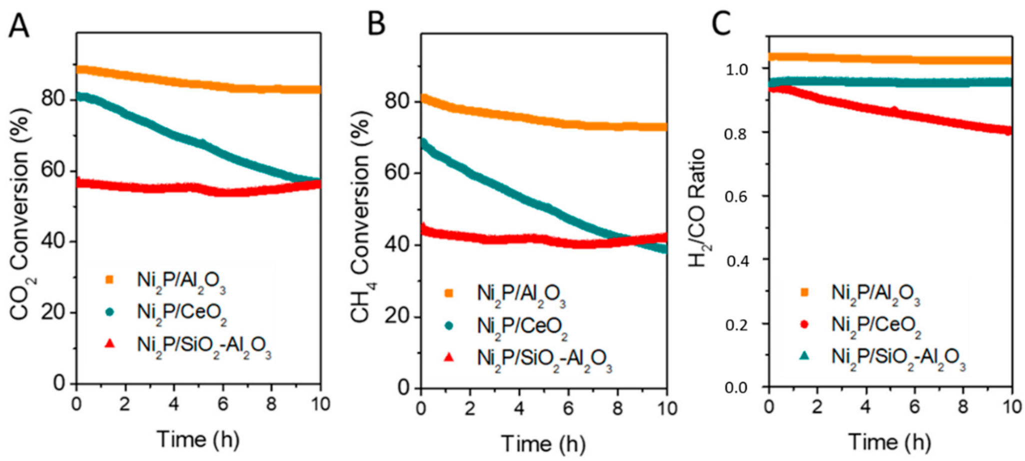


**Figure 4.** Catalytic performance exhibited by the catalysts' series at 30 L/g·h and feed composition $N_2/CO_2/CH_4$—50/25/25. (**A**) $CO_2$ conversion; (**B**) $CH_4$ conversion and (**C**) $H_2/CO$ ratio.

The reaction rate observed for the catalysts' series decreased according to the sequence: $Ni_2P/Al_2O_3$ > $Ni_2P/CeO_2$ > $Ni_2P/SiO_2$-$Al_2O_3$. Thus, the highest $CO_2$ conversion, combined with good catalyst stabilities, revealed the $Ni_2P/Al_2O_3$ system as the best-performing catalyst. On the contrary, the worst catalyst behaviour of the series was exhibited by the $Ni_2P/SiO_2\_Al_2O_3$ catalyst. The lower conversion rates might be associated to important cooking processes over such acidic surfaces. Rather unexpected poor catalytic behaviours were displayed by $Ni_2P/CeO_2$ catalysts. Thus, even though relatively optimal catalyst performances were initially depicted, the $Ni_2P/CeO_2$ catalyst depicted an important loss of catalytic activity, with the $CO_2$ conversion dropping from around 80 to 50% and the $CH_4$ conversion dropping from around 70 to 35% during the catalytic test. For this sample, the significantly lower catalyst surface area could be related to the deprived catalyst performance.

### 2.4. XRD of the Spent Samples

Considering the importance of deactivation issues related to sintering or coking processes described for DRM catalysts [27], a glimpse into the catalyst structural variations attained over the different samples under reaction conditions was attempted through XRD analysis. Figure 5 shows the diffractograms obtained for the post-reacted samples. For $Ni/CeO_2$ catalysts, no diffraction lines associated to Ni phases were discerned. In agreement with XPS data, ceria support seems, indeed, to favour higher Ni metal dispersions [6]. For $Ni/Al_2O_3$ and $Ni_2P/SiO_2$-$Al_2O_3$ catalysts, diffraction lines associated to the $Ni^0$ phase were clearly evidenced. Still, despite the good dispersions observed for the reduced sample, the spent $Ni_2P/SiO_2$-$Al_2O_3$ sample showed prominent $Ni^0$ diffraction peaks, indicating that significantly larger Ni crystal sizes were constituted by the $Ni_2P/SiO_2$-$Al_2O_3$ catalyst under reactions conditions. The higher Ni particles observed for the $SiO_2$-$Al_2O_3$ catalyst suggest that, despite the relatively high metal dispersions obtained with silica-based catalysts, poor resistances against sintering issues are presented. Moreover, the $Ni/Al_2O_3$ sample exhibited clear diffraction peaks at 41.5°, ascribed to $Ni_2P$ phases (JCPDS No. 01-074-1385), whilst a small $Ni_2P$ contribution could also be intuited for the $Ni_2P/SiO_2$-$Al_2O_3$ catalyst sample. The larger concentration of $Ni_2P$ species, constituted for the $Ni/Al_2O_3$ catalyst, agrees with the findings provided by XPS data.

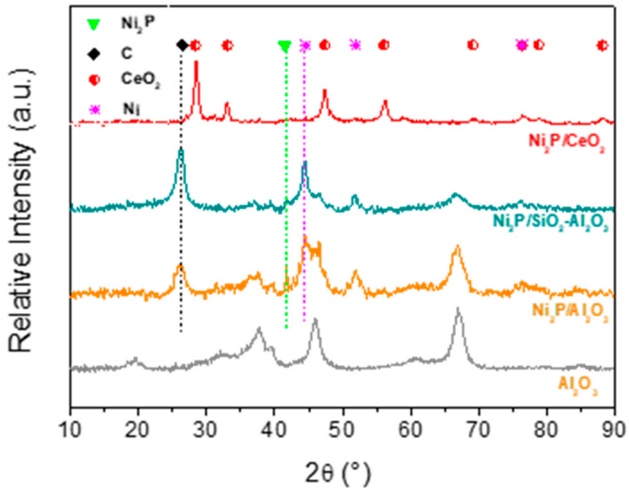


**Figure 5.** XRD diffractograms obtained for the spent catalysts.

In respect to carbon deposits, both the $Ni/Al_2O_3$ and $Ni_2P/SiO_2$-$Al_2O_3$ samples exhibited evident diffraction lines placed at 26.5° associated to structured carbon phases (JCPDS No. 75-1621), evidencing the constitution of coke deposits under reaction atmospheres. Comparatively, significantly larger amounts of C deposits were constituted over the silica supported catalyst. Given the higher surface acidity of silica-doped alumina [27], promoted deactivation processes related to coking phenomena are, indeed, expected [28,29]. In any case, carbon-forming reactions are, indeed, thermodynamically favoured for large nickel crystallites [30,31]. Therefore, the larger Ni particle sizes, combined with the intrinsic acidity of silica surfaces, account for the significantly higher amounts of carbon deposits constituted and for the observed conversion drop during the catalytic test. On the contrary, the absence of C related peaks for the $Ni/CeO_2$ catalyst suggest the active role of ceria support against the constitution of carbon deposits.

Overall, the behaviour observed for the catalysts' series evidences $Al_2O_3$ support as the right choice for $Ni_2P$ catalysts in DRM reactions. For $CO_2$ methanation, higher concentrations of $Ni_2P$ were also related to improved reaction rates over $Al_2O_3$ supported systems [24]. Along with promoted $CO_2$ activations, the perturbed electronic structure achieved within $Ni_2P$ has been proposed to increase the resistance against deactivation effects related to Ni oxidation [32] and carbon deposits [33]. Thus, the optimal activity and stability depicted by the $Ni_2P/Al_2O_3$ catalyst could be associated to the significant highest fractions of $Ni_2P$ species present on the catalyst surface, coupled with fair and relatively stable Ni dispersions. In a similar manner, the lower catalytic behaviour observed for the $Ni_2P/SiO_2$-$Al_2O_3$ system should be associated with larger Ni agglomerates along with the lower $Ni_2P$ concentrations observed over the catalyst surface. Besides, the larger coke deposits found on the $Ni_2P/SiO_2$-$Al_2O_3$ catalyst surface might also deplete its catalyst performance and propensity towards the development of carbon deposits due to the large Ni agglomerates dispersed over highly acidic surfaces. Moreover, the lower DRM performance observed for the Ni/$CeO_2$ catalyst might be strongly affected by the lower surface areas depicted by this sample. For the ceria supported sample, the strong interaction established between Ni and $CeO_2$ supports might hinder the effective constitution of $Ni_2P$ phosphide species. In any case, Ni-O-Ce sites are suggested to be active for the total oxidation of methane [34], with the evolution of $CO_2$ molecules formed through the reaction between hydroxyls groups constituted over $Ce^{3+}$ sites and surface methyl groups [35]. The relatively lower catalytic performances displayed by the Ni/$CeO_2$ sample could also be associated with favoured methane oxidation reactions. The absence of carbon deposits and Ni sintering effects evidenced in the XRD analysis of the post-reacted samples suggest the constitution of $Ni^{2+}$ species, inactive for $CO_2$ activation, as the main deactivation cause.

## 3. Materials and Methods

### *3.1. Catalyst Synthesis*

All three catalysts were prepared by impregnation of the relevant support with a nickel phosphate solution. For that purpose, $\gamma$-$Al_2O_3$ and 20% $SiO_2$-80% $Al_2O_3$ (Puralox SCFa-230 and Siralox 20/380, Sasol, Johannesburg, South Africa) commercial supports were employed. A third home-made ceria support was also employed. Then, $CeO_2$ support was synthesised by the reaction of urea and cerium nitrate. Thus, adequate amounts were dissolved in 100 mL of deionised water. After being stirred at 85 °C for 24 h, the solution was then filtered to collect the precipitate, which was dried overnight at 80 °C. The obtained solid was calcined in air at 400 °C for 4 h to produce a $CeO_2$ powder.

The nickel phosphide catalysts were prepared by a procedure similar to that seen in the literature [36,37]. Thus, the intended nominal contents were 20%Ni and had a Nickel:Phosphorous molar ratio of 3:2. For that purpose, a nickel phosphate solution was prepared by mixing solutions of $Ni(NO_3).6H_2O$ and $(NH_4)_2HPO_4$ in deionised water, producing a nickel phosphate precipitate. The nickel phosphate solution was impregnated over the chosen supports and the excess of solvent was removed by rotary vacuum evaporation. The obtained samples were in an oven at 80 °C and calcined in air at 500 °C for 4 h. Over Puralox SCFa-230, Siralox 20/380 and $CeO_2$ supports, the obtained catalysts were labelled $Ni_2P/Al_2O_3$, $Ni_2P/SiO_2$-$Al_2O_3$ and $Ni_2P/CeO_2$, correspondingly. In agreement with previous works [36,37], $Ni_2P$ structures were constituted after subsequent reductions in $H_2$ presence.

### *3.2. Catalyst Characterisation*

The textural properties of the samples were analysed using $N_2$ adsorption at −196 °C on an Autosorb iQ Station 2 instrument (Anton Paar QuantaTec Inc., Boynton Beach, FL, USA). The weight-specific surface area of the catalysts was determined using the Brunauer–Emmett–Teller equation [11]; the average pore size and weight-specific pore volume were calculated using the Barett–Joyner–Halenda method [22].

X-ray diffraction analysis was carried out on Panalytical X'Pert Pro Powder equipment (Marvern Panalytical) using Cu K$\alpha$ radiation at 30 mA and 40 kV. X-ray photoelectron spectra were collected in order to determine the composition of the catalysts' surfaces using a K-Alpha Thermo Scientific instrument. The XPS analysis was carried out on freshly reduced catalysts. The spectra were recorded using Al-K radiation at 1486.6 eV, which was monochromatised by a twin crystal monochromator to produce a focused elliptical X-ray spot with a major axis length of 400 µm. The initial survey was carried out from a binding energy of 1350 eV to 0 eV, with higher resolution detailed scans being taken of the most relevant sections.

### *3.3. Catalyst Reaction Testing*

The catalysts were tested at atmospheric pressure in a 10 mm internal diameter quartz tube reactor. In these tests, the reactor was loaded with 0.1 g of catalyst and fed with 100 mL/min of 50 vol.% $N_2$, 25 vol.% $CO_2$ and 25 vol.% $CH_4$; neglecting the inert nitrogen, the Weight Hourly Space Velocity (WHSV) was 30 $L \cdot g^{-}1 \cdot h^{-1}$. Prior to reaction testing, the catalysts were reduced in a 10 vol.% hydrogen stream with nitrogen as an inert carrier at 800 °C for 1 h. The gas mixture compositions were evaluated with an ABB continuous gas analyser (model ABB AO2020). The $CO_2$ and $CH_4$ conversions were estimated according to Equations (1) and (2), respectively.

$$\text{Conversion of } CO_2(\%) = 100 \times \frac{[CO_2]_{in} - [CO_2]_{out}}{[CO_2]_{in}} \quad (1)$$

$$CH_4 \text{ Conversion } (\%) = 100 \times \frac{[CH_4]_{in} - [CH_4]_{out}}{[CH_4]_{in}} \quad (2)$$

## 4. Conclusions

In this work, the catalytic performance of supported nickel phosphide catalysts was investigated for dry reforming of methane. By analysing $Al_2O_3$, $SiO_2$-$Al_2O_3$ and $CeO_2$ supports, the prominent impact of the support nature on the catalytic behaviour of $Ni_2P$ systems was clearly established. The reaction rate observed for the catalysts' series decreased, following the trend $Ni_2P/Al_2O_3$ > $Ni_2P/CeO_2$ > $Ni_2P/SiO_2$-$Al_2O_3$. The observed catalytic trend should be explained considering different factors. Thus, lower conversion rates, depicted by the $Ni_2P/SiO_2$-$Al_2O_3$ system, were related to the higher Ni sintering and coking rates, coupled with hindered constitutions of $Ni_2P$ species. For the $Ni_2P/CeO_2$ system, the lower surface areas coupled with low concentrations of $Ni_2P$ constituted over the catalyst surface might account for the exhibited catalytic performance. In any case, the strong deactivation issues displayed by the $Ni_2P/CeO_2$ catalyst under reaction conditions should most likely relate to the partial oxidation of Ni species, since no significant C deposits nor Ni sintering effects were discerned for the post-reacted sample. For the ceria supported catalysts, the oxidation of methane and C intermediate species might also play a role.

Therefore, the obtained outcomes suggest the unsuitability of $Ni_2P/CeO_2$ and $Ni/SiO_2$-$Al_2O_3$ catalysts for DRM processes. Within the analysed series, the $Ni_2P/Al_2O_3$ catalyst showed the highest catalyst performance as well as excellent stabilities. At 700 °C, the alumina supported catalyst consistently produced stable $CO_2$ conversions only 12% below equilibrium and a favourable $H_2/CO$ ratio of 1. The observed catalyst behaviour could be associated to the larger concentrations of $Ni_2P$ phases and fair Ni dispersions. Overall, the $Ni_2P/Al_2O_3$ catalyst has been proven to be an effective and easily synthesised novel catalyst with remarkable activity and stability for DRM reaction.

**Author Contributions:** M.G.-C.: writing—original draft preparation, writing—review and editing, visualization; E.l.S.: data curation, investigation, formal analysis, methodology; C.B.: data curation, investigation; L.P.-P.: investigation, supervision, methodology; H.A.-G.: conceptualization; Q.W.: data analysis, writing—editing, methodology; T.R.R.: conceptualization, project administration, funding acquisition. All authors have read and agreed to the published version of the manuscript.

**Funding:** The team at Surrey acknowledges the financial support provided by the EPSRC grant EP/R512904/1 as well as the Royal Society Research Grant RSGR1180353. This work was also partially sponsored by the CO2Chem UK through the EPSRC grant EP/P026435/1.

**Data Availability Statement:** The data described in this article are openly available in the Open Science Frameworks at Digital Repositories of the University of Surrey (ExLibris) and Branden-burg University of Technology (OPUS).

**Acknowledgments:** The authors acknowledge to Sasol for kindly providing the materials.

**Conflicts of Interest:** The authors declare no conflict of interests.

## References


1. Aminu, M.D.; Nabavi, S.A.; Rochelle, C.A.; Manovic, V. A Review of Developments in Carbon Dioxide Storage. *Appl. Energy* **2017**, *208*, 1389–1419. [CrossRef]
2. Pakhare, D.; Spivey, J. A review of dry ($CO_2$) reforming of methane over noble metal catalysts. *Chem. Soc. Rev.* **2014**, *43*, 7813–7837. [CrossRef] [PubMed]
3. Boehman, A.L.; Le Corre, O. Combustion of syngas in internal combustion engines. *Combust. Sci. Technol.* **2008**, *180*, 1193–1206. [CrossRef]
4. Dry, M.E. The Fischer-Tropsch process: 1950–2000. *Catal. Today* **2002**, *71*, 227–241. [CrossRef]
5. Ganesh, I. Conversion of carbon dioxide into methanol-A potential liquid fuel: Fundamental challenges and opportunities (a review). *Renew. Sustain. Energy Rev.* **2014**, *31*, 221–257. [CrossRef]
6. Arora, S.; Prasad, R. An overview on dry reforming of methane: Strategies to reduce carbonaceous deactivation of catalysts. *RSC Adv.* **2016**, *6*, 108668–108688. [CrossRef]
7. Dębek, R.; Motak, M.; Grzybek, T.; Galvez, M.E.; Da Costa, P. A short review on the catalytic activity of hydrotalcite-derived materials for dry reforming of methane. *Catalysts* **2017**, *7*, 1–25. [CrossRef]
8. Stroud, T.; Smith, T.J.; Le Saché, E.; Santos, J.L.; Centeno, M.A.; Arellano-Garcia, H.; Odriozola, J.A.; Reina, T.R. Chemical $CO_2$ recycling via dry and bi reforming of methane using Ni-Sn/$Al_2O_3$ and Ni-Sn/$CeO_2$-$Al_2O_3$ catalysts. *Appl. Catal. B Environ.* **2018**, *224*, 125–135. [CrossRef]
9. Wang, Y.; Yao, L.; Wang, S.; Mao, D.; Hu, C. Low-temperature catalytic $CO_2$ dry reforming of methane on Ni-based catalysts: A review. *Fuel Process. Technol.* **2018**, *169*, 199–206. [CrossRef]
10. Liu, P.; Rodriguez, J.A. Catalysts for hydrogen evolution from the [NiFe] hydrogenase to the Ni 2P(001) surface: The importance of ensemble effect. *J. Am. Chem. Soc.* **2005**, *127*, 14871–14878. [CrossRef]
11. Korányi, T.I.; Vít, Z.; Poduval, D.G.; Ryoo, R.; Kim, H.S.; Hensen, E.J.M. SBA-15-supported nickel phosphide hydrotreating catalysts. *J. Catal.* **2008**, *253*, 119–131. [CrossRef]
12. Porosoff, M.D.; Yang, X.; Boscoboinik, J.A.; Chen, J.G. Molybdenum carbide as alternative catalysts to precious metals for highly selective reduction of $CO_2$ to CO. *Angew. Chemie Int. Ed.* **2014**, *53*, 6705–6709. [CrossRef]
13. Liu, P.; Rodriguez, J.A. Water-gas-shift reaction on molybdenum carbide surfaces: Essential role of the oxycarbide. *J. Phys. Chem. B* **2006**, *110*, 19418–19425. [CrossRef]
14. Yao, Z.; Luan, F.; Sun, Y.; Jiang, B.; Song, J.; Wang, H. Molybdenum phosphide as a novel and stable catalyst for dry reforming of methane. *Catal. Sci. Technol.* **2016**, *6*, 7996–8004. [CrossRef]
15. Guharoy, U.; Ramirez Reina, T.; Gu, S.; Cai, Q. Mechanistic insights into selective $CO_2$ Conversion via RWGS on Transition Metal Phosphides: A DFT Study. *J. Phys. Chem. C* **2019**, *123*, 22918–22931. [CrossRef]
16. Liu, P.; Rodriguez, J.A.; Takahashi, Y.; Nakamura, K. Water-gas-shift reaction on a Ni2P(001) catalyst: Formation of oxy-phosphides and highly active reaction sites. *J. Catal.* **2009**, *262*, 294–303. [CrossRef]
17. Sawhill, S.J.; Phillips, D.C.; Bussell, M.E. Thiophene hydrodesulfurization over supported nickel phosphide catalysts. *J. Catal.* **2003**, *215*, 208–219. [CrossRef]
18. Guharoy, U.; Ramirez Reina, T.; Olsson, E.; Gu, S.; Cai, Q. Theoretical Insights of Ni2P (0001) Surface toward Its Potential Applicability in $CO_2$ Conversion via Dry Reforming of Methane. *ACS Catal.* **2019**, *9*, 3487–3497. [CrossRef]
19. Zhang, Q.; Pastor-Pérez, L.; Jin, W.; Gu, S.; Reina, T.R. Understanding the promoter effect of Cu and Cs over highly effective B-Mo2C catalysts for the reverse water-gas shift reaction. *Appl. Catal. B Environ.* **2019**, *244*, 889–898. [CrossRef]
20. Gonzalez-Castano, M.; Miguel Navarro De, J.C.; Sinha, F.; Wabo, S.G.; Klepel, O.; Arellano-garcia, H. Cu supported Fe-$SiO_2$ nanocomposites for reverse water gas shift reaction. *J. $CO_2$ Util.* **2021**, *46*, 101493. [CrossRef]
21. Omar, F.S.; Numan, A.; Duraisamy, N.; Bashir, S.; Ramesh, K.; Ramesh, S. Ultrahigh capacitance of amorphous nickel phosphate for asymmetric supercapacitor applications. *RSC Adv.* **2016**, *6*, 76298–76306. [CrossRef]
22. Brunauer, B.S.; Emmett, P.H. Adsorption of gases in multimolecular layers. *J. Am. Chem. Soc.* **1938**, *60*, 309–319. [CrossRef]
23. Xin, H.; Guo, K.; Li, D.; Yang, H.; Hu, C. Production of high-grade diesel from palmitic acid over activated carbon-supported nickel phosphide catalysts. *Appl. Catal. B Environ.* **2016**, *187*, 375–385. [CrossRef]
24. Zhang, L.; Ren, X.; Guo, X.; Liu, Z.; Asiri, A.M.; Li, B.; Chen, L.; Sun, X. Efficient Hydrogen Evolution Electrocatalysis at Alkaline pH by Interface Engineering of Ni 2 P—$CeO_2$. *Inorg. Chem.* **2018**. [CrossRef]
25. Suib, S.L.; Winiecki, A.M.; Kostapapas, A. Surface states of aluminophosphate and zeolite molecular sieves. *Stud. Surf. Sci. Catal.* **1986**, *28*, 409–414. [CrossRef]
26. Anh, P.; Cam, N.; Luu, L.; Van Nguyen, T.T.; Nguyen, T.; Cuong, T. Improving the performance of nickel catalyst supported on mesostructured silica nanoparticles in methanation of $CO_2$-rich gas by urea–nitrate combustion. *Chem. Pap.* **2020**, *74*, 3925–3935. [CrossRef]
27. Wei, J.; Iglesia, E. Isotopic and kinetic assessment of the mechanism of reactions of $CH_4$ with $CO_2$ or $H_2O$ to form synthesis gas and carbon on nickel catalysts. *J. Catal.* **2004**, *224*, 370–383. [CrossRef]
28. Li, S.; Gong, J. Strategies for improving the performance and stability of Ni-based catalysts for reforming reactions. *Chem. Soc. Rev.* **2014**, *43*, 7245–7256. [CrossRef] [PubMed]
29. Kroll, V.C.H.; Swaan, H.M.; Lacombe, S.; Mirodatos, C. Methane reforming reaction with carbon dioxide over Ni/$SiO_2$ catalyst: II. A mechanistic study. *J. Catal.* **1996**, *164*, 387–398. [CrossRef]

30. Liang, W.; Yan, H.; Chen, C.; Lin, D.; Tan, K.; Feng, X.; Liu, Y.; Chen, X.; Yang, C.; Shan, H. Revealing the effect of nickel particle size on carbon formation type in the methane decomposition reaction. *Catalysts* **2020**, *10*, 890. [CrossRef]
31. Wang, H.Y.; Ruckenstein, E. Conversions of methane to synthesis gas over Co/$\gamma$-$Al_2O_3$ by $CO_2$ and/or $O_2$. *Catal. Lett.* **2001**, *75*, 13–18. [CrossRef]
32. Liu, P.; Rodriguez, A.; Asakura, T. Desulfurization Reactions on Ni2P (001) and α-Mo2C (001) Surfaces: Complex Role of P and C Sites. *J. Phys. Chem. B* **2005**, *109*, 4575–4583. [CrossRef]
33. Wang, Z.; Cao, X.; Zhu, J.; Hu, P. Activity and coke formation of nickel and nickel carbide in dry reforming: A deactivation scheme from density functional theory. *J. Catal.* **2014**, *311*, 469–480. [CrossRef]
34. Kim, D.K.; Stöwe, K.; Müller, F.; Maier, W.F. Mechanistic study of the unusual catalytic properties of a new Ni—Ce mixed oxide for the $CO_2$ reforming of methane. *J. Catal.* **2007**, *247*, 101–111. [CrossRef]
35. Xu, W.; Liu, Z.; Johnston-Peck, A.C.; Senanayake, S.D.; Zhou, G.; Stacchiola, D.; Stach, E.A.; Rodriguez, J.A. Steam reforming of ethanol on Ni/$CeO_2$: Reaction pathway and interaction between Ni and the $CeO_2$ support. *ACS Catal.* **2013**, *3*, 975–984. [CrossRef]
36. Wagner, J.L.; Jones, E.; Sartbaeva, A.; Davis, S.A.; Torrente-Murciano, L.; Chuck, C.J.; Ting, V.P. Zeolite y supported nickel phosphide catalysts for the hydrodenitrogenation of quinoline as a proxy for crude bio-oils from hydrothermal liquefaction of microalgae. *Dalt. Trans.* **2018**, *47*, 1189–1201. [CrossRef] [PubMed]
37. Yun, G.; Guan, Q.; Li, W. The synthesis and mechanistic studies of a highly active nickel phosphide catalyst for naphthalene hydrodearomatization. *RSC Adv.* **2017**, *7*, 8677–8687. [CrossRef]